



The key regulator circPDE3B promotes arsenic-induced bladder carcinogenesis by affecting STAT3 and NF- κ B stability

Yihong Gao · Haotian Xu · Qingyun Zhao · Dunyu Cai · Xiaodong Zhou · Xingcai Chen · Shengyi Yuan · Deqing Li · Taoran Ning · Xiangyu Dong · Mengyao Li · Gang Li · Aruo Nan

Received: 28 November 2024 / Accepted: 9 May 2025
© The Author(s) 2025

Abstract Long-term exposure to arsenic (As), which is a ubiquitous environmental contaminant, significantly enhances the risk of multiple cancers, including bladder and lung cancers. In recent years, the important roles of circular RNAs (circRNAs) in tumorigenesis and development have attracted widespread attention. However, the specific molecular mechanisms by which circRNAs promote bladder cancer development following exposure to arsenic remain incompletely understood. This study is the first to demonstrate that circPDE3B is significantly upregulated in a cell model of transformation

triggered by arsenic and that it promotes this transformation process. Our study elucidated the biological function of circPDE3B in vitro, in SV-HUC-1 cells, showing that it accelerates the malignant transformation from arsenic via increasing cell proliferation and inhibiting apoptosis. Furthermore, we delineated a novel molecular mechanism whereby circPDE3B directly binds to NF- κ B and STAT3, inhibiting their ubiquitination and increasing their stability. This, in turn, affects downstream HIF-1 α expression, promoting the malignant transformation of SV-HUC-1 cells and eventually resulting in bladder carcinogenesis. Our research reveals the critical regulatory role of circPDE3B in the arsenic-triggered malignant transformation within SV-HUC-1 cells. This study offers broader perspectives on the molecular mechanisms driving bladder cancer progression, while also identifying potential targets for early diagnosis and treatment of bladder tumour.

Yihong Gao and Haotian Xu contributed equally to this work.

Supplementary Information The online version contains supplementary material available at <https://doi.org/10.1007/s10565-025-10038-2>.

Y. Gao · H. Xu · Q. Zhao · D. Cai · X. Zhou · X. Chen · S. Yuan · D. Li · T. Ning · X. Dong · M. Li · G. Li (✉) · A. Nan (✉)
School of Public Health, Guangxi Medical University, Nanning 530021, China
e-mail: ligang@gxmu.edu.cn

A. Nan
e-mail: nanaruo@163.com

Y. Gao · H. Xu · Q. Zhao · D. Cai · X. Zhou · X. Chen · S. Yuan · D. Li · T. Ning · X. Dong · M. Li · G. Li · A. Nan
Guangxi Key Laboratory of Environment and Health Research, Guangxi Medical University, Nanning 530021, China

Keywords Arsenic · Bladder cancer · circPDE3B · NF- κ B · STAT3

Introduction

Arsenic is prevalent in the environment and primarily enters the body through drinking water, food and air; arsenic has been classified as a class I carcinogen by the International Agency for Research on Cancer. Epidemiological evidence has suggested that arsenic

exposure significantly contributes to bladder cancer incidence (Byeon et al. 2021; Sassano et al. 2023; Speer et al. 2023; Virk et al. 2023). Arsenic can induce bladder cancer development through genetic mechanisms, including by triggering DNA damage and chromosomal aberrations (Kurosawa et al. 2023; Mehus et al. 2022; Muenyi et al. 2015). In addition, arsenic promotes the carcinogenesis of bladder cancer through epigenetic mechanisms, such as DNA methylation and histone modification (Chang et al. 2019; Porten 2018; Tryndyak et al. 2020). Nonetheless, the molecular mechanisms by which arsenic triggered bladder carcinogenesis have not been fully elucidated. With the rapid evolution of high-throughput sequencing methods, the roles of circular RNAs (circRNAs) as novel epigenetic regulators of carcinogenesis have attracted widespread attention.

circRNAs are a type of closed, covalent-circular RNA molecules that are characterized with high stability, high conservation and tissue specificity (Chen and Shan 2021; Kristensen et al. 2022). Current findings reveal that circular RNAs exert critical functions in bladder carcinogenesis by modulating multiple biological processes. For example, circHIPK3 serves as a miRNA sponge for miR-558, inhibiting the invasion, migration and angiogenesis of bladder tumour cells (Li et al. 2022b); additionally, circXRN2 prevents the SPOP-mediated degradation of LATS1 through competitive inhibition, thereby activating the Hippo signaling pathway (Xie et al. 2023). Research on the roles of circRNAs in arsenic-induced bladder carcinogenesis is still lacking. However, exogenous chemicals can lead to circRNA differential expression, which in turn regulates key tumour factors, causes changes in cellular function, and ultimately affects tumorigenesis and progression (Li et al. 2023a; Liu et al. 2024b; Qiu et al. 2022; Wang et al. 2024).

STAT3 and NF- κ B are common transcriptional activators in tumours and play important roles in regulating various aspects of cell proliferation, apoptosis, angiogenesis, and immune escape. STAT3 controls numerous genes upon activation (Dong et al. 2021; Li et al. 2023b; Zou et al. 2020), whereas NF- κ B is a core mediator of both natural and specific immune responses that functions primarily in response to inflammatory and stress-related signals (Guldenpfennig et al. 2023; Guo et al. 2024; Poma 2020). Numerous studies have reported abnormal activation patterns of these transcriptional regulators

in diverse neoplasms, especially in bladder cancer (Amara et al. 2024; Wu et al. 2021; Yu et al. 2020). For example, BUB1 kinase drives bladder cancer progression and proliferation by regulating STAT3 transcription (Jiang et al. 2021); in bladder cancer, USP24-GSDMB complex formation stimulates cell proliferation via STAT3-dependent mechanisms (He et al. 2021); ROC1 gives rise to bladder cancer malignancy via orchestrating NF- κ B signaling activation (Wu et al. 2021); Mechanistic studies reveal that secretory granule protein II facilitates bladder cancer advancement by concurrently activating both MAPK and NF- κ B pathways (Zhou et al. 2024). Therefore, exploring the regulatory patterns of circRNAs that target both STAT3 and NF- κ B will help elucidate the potential mechanism underlying arsenic-induced bladder cancer.

In our research, we successfully established a model about malignant transformation triggered via chronic arsenic exposure in SV-HUC-1 cells. The circRNA circPDE3B, which is highly expressed in bladder cancer, was screened via genome-wide circRNA screening, and circPDE3B was found to be chronically elevated during the arsenic-induced oncogenic conversion of SV-HUC-1 cells. Functionally, circPDE3B potentiated the progression of arsenic-induced SV-HUC-1 cell malignant transformation by promoting cell proliferation and inhibiting apoptosis. Mechanistically, circPDE3B targeted the key tumour factors STAT3 and NF- κ B, inhibited their ubiquitination, and increased their stability, which in turn upregulated the transcriptional level expression of HIF-1 α and ultimately promoted bladder carcinogenesis. In conclusion, our study demonstrated that circPDE3B serves as a pivotal regulator in arsenic-induced bladder carcinogenesis, uncovering previously unrecognized mechanisms of arsenic-induced bladder carcinogenesis from an epigenetic perspective.

Materials and methods

Cell culture

Immortalized human ureteral epithelial cells (SV-HUC-1) (Cellcook, CC4009) and embryonic kidney cells (293 T cells) [American Type Culture Center (ATCC)] were used in this study. SV-HUC-1 cells were grown using Ham's F-12 K complete medium

[10% foetal bovine serum (Gibco, 10099141C) and 1% streptomycin/penicillin (Servicebio, G4003)]. Embryonic kidney cells (293 T cells) were cultured in complete DMEM [10% foetal bovine serum (Gibco, 10099141C) and 1% streptomycin/penicillin (Servicebio, G4003)]. All the cell lines were cultured at 37 °C in a 5% CO₂ incubator at a constant temperature.

Establishment of a malignantly transformed cell model

SV-HUC-1 cells were grown in Ham's F-12 K complete medium with the addition of 0.5 µM NaAsO₂ for 48 h (37 °C, 5% CO₂). After the cells attained 80%–90% density, the cells were passaged and then cultured via the method described above, with continuous exposure to NaAsO₂ for 80 generations. The degree of malignant transformation of the cells was determined with a soft agar colony formation assay.

CCK-8 assay

Cells were seeded in 96-well plates at a density of 1×10^4 cells/well and cultured under standard conditions (37 °C, 5% CO₂). After the cells had completely attached to the well, cell viability was assessed with a CCK-8 Cell Viability Reagent Kit (Dojindo, CK04); in brief, the CCK-8 reagent was diluted in complete medium at a ratio of 1:10, added to the wells of interest (divided into an experimental group, a control group and a blank group), and incubated at 37 °C in a constant-temperature incubator for 60 min. The absorbance at 450 nm was measured with an enzyme marker.

Real-time fluorescence quantitative PCR (RT-qPCR) assay

Total RNA was extracted from cells with TRIzol reagent (Invitrogen, 15596018), and the concentration of the purified total RNA was determined with an ultramicro-UV spectrophotometer (Thermo Fisher Scientific). The RNA was reverse transcribed to cDNA with the GoScript™ Reverse Transcription System Kit (Promega, A5001). cDNA was performed using GoTaq qPCR Master Mix (Promega, A6001) in an Applied Biosystems QuantStudio 7 Flex Real-Time PCR System (Thermo Fisher Scientific) and

subjected to quantitative PCR analysis. GAPDH or U6 served as endogenous controls for data normalization, the primers were commercially obtained from Sangon Biotech, and gene expression quantification was performed through with the $2^{-\Delta\Delta Ct}$ method. Primer nucleotide sequences are shown in Table S1.

Linear digestive enzyme assay

Total RNA was performed, followed by treatment with 3 U/µg of RNase R. RNA digestion was conducted under controlled conditions (37 °C water bath) for 10 min. Moreover, genomic DNA (gDNA) was carried out using a gDNA extraction kit (Invitrogen, K1820) and immediately placed on ice for stabilization. Finally, the samples before and after RNase R treatment and the gDNA samples were used for to PCR amplification with circPDE3B-specific polymeric and divergent primers, after which agarose gel electrophoresis was carried out to verify the circular structure of circPDE3B.

RNA stability experiment

SV-HUC-1 cells were seeded in six-well plates at a concentration of 3×10^5 cells/well. Upon attaining 90% confluency, total cellular RNA was extracted and subjected to RT-qPCR analysis to assess mRNA expression following exposure to 2 µg/ml actinomycin D at 0 h, 4 h, 8 h, and 16 h.

Stable silencing and overexpression of circPDE3B in cell lines

Specific primers were designed according to the circPDE3B sequence, and after PCR amplification, plasmids for the stable silencing or overexpression of circPDE3B were constructed with a stable silencing vector (pLVX-shRNA2-puro) and a stable overexpression vector (pLV-puro-GFP-circRNA-1) were purchased from IEMed and BersinBio. Lentiviral packaging was carried out using 293 T cells, and the filtered viral supernatants were used to infect SV-HUC-1 cells for 48 h. Images were obtained using a fluorescence microscopy, and puromycin (2 µg/ml) was employed to single out the stable cells lines in which circPDE3B was silenced or overexpressed.

EdU incorporation assay

Cell suspensions (1×10^4 cells/well) were seeded in 96-well, and the nuclei were stained with DAPI with the EdU Cell Proliferation Detection Kit (RiboBio, C10310-1). The cells that were in the proliferative phase were labelled with EdU. Subsequently, images of cell fluorescence were captured with the EVOS FL Automated Imaging System, and the ability of their proliferation was quantified by ImageJ analysis software.

Cell cycle detection by flow cytometry

Cells were seeded in 6-well culture dishes at a concentration of 3×10^5 cells/well. Once the cells reached 90% confluence, they were washed with PBS, trypsin was introduced, after which the cells were collected through centrifugation-induced precipitation. Then, anhydrous ethanol and PBS were mixed at a 7:3 ratio, and the cells were resuspended in this mixture and fixed at 4°C overnight. Subsequently, the RNase A enzyme from a cell cycle kit (KeyGen BioTECH, KGA9101) was added, and following a period of incubation for 30 min at 37°C , PI solution was added and kept in the dark at 4°C for 30 min. The cell cycle was subsequently analysed via CytoFLEX flow cytometry (Beckman Coulter), and the G0/G1 phase as well as the G2/M phase cell ratios were subsequently analysed and compared.

Flow cytometry analysis for apoptosis detection

Cells were seeded in 6-well plates at a density of 3×10^5 cells/well, and upon reaching 90% confluence, the cell supernatants were collected, the cells were digested using EDTA-free trypsin, followed by collection and centrifugation. The collected cells were subsequently stained with Annexin V-APC and PI with an Annexin V-APC/PI Apoptosis Detection Kit (KeyGen BioTECH, KGA1107), and apoptosis was detected with a CytoFLEX flow cytometer (Beckman Coulter). Finally, the proportions of early apoptotic and late apoptotic cells were statistically analysed and compared between the groups.

Soft agar colony formation assay

Soft agar was formed with a formulation of $2 \times$ BME medium (Sigma, B9638): foetal bovine serum (Zhejiang Tianhang Technology Co., Ltd., 13011-8611): $1 \times$ PBS (Servicebio, G4207): $100 \times$ double antibody (Servicebio, G4003): $100 \times$ glutamine (Gibco, A2916801): 7.5% sodium carbonate solution (Gibco, 25080094) at a 4:1:1:0.1:0.1:0.1 ratio and set aside, and subsequently, medium and agar gel (1.25%) were added to six-well plates (3 ml/well) at a proportion of 3:2 and permitted to solidify at room temperature for 3 h. Subsequently, a cell suspension of 1×10^4 cells/well was prepared and mixed with medium and agar gel, added to six-well plates within a volume of 1 ml of medium per well, and allowed to solidify at room temperature. Then, the plates were incubated at 37°C in a 5% CO_2 incubator for 20 days, and then, colony formation was observed under a microscope.

Nucleoplasmic separation assay

First, 3×10^6 SV-HUC-1 cells were collected, and the nuclear and cytoplasmic components were isolated using the PARIS™ Kit (Invitrogen, AM1921). Then, samples were collected to measure the nuclear RNA concentration and the cytoplasmic RNA concentration, respectively, with an Ultra-Micro UV Spectrophotometer (Thermo Fisher Scientific). After reverse transcription of the RNA to cDNA, the distribution of circPDE3B between the nucleus and cytoplasm was quantitatively assessed using qPCR, in which GAPDH was used as the cytoplasmic reference and U6 used as the cytosolic control, and the results were statistically analysed.

Fluorescence in situ hybridization (FISH)

Specific FISH probes were designed based on the circPDE3B sequence, and the sequence information is detailed in Table S1. A total of 1×10^4 SV-HUC-1 cells were seeded in 12-well plate crawler slices, and when the cells had reached 70% confluence, the cells were fixed, permeabilized and dehydrated. After that, the cells were subjected to probe hybridization and DAPI staining according to the FISH kit (RiboBio, C10910). Ultimately, the cells were imaged using a confocal microscope (Zeiss).

RNA immunoprecipitation (RIP)

A total of 1×10^7 SV-HUC-1 cells were collected, and experiments were conducted using a RIP detection kit (IEMed, K303). First, antibody-protein A/G complexes were prepared, an anti-NF- κ B and anti-STAT3 antibody was added as bait protein to the IP group, an IgG antibody was mixed to the IgG group, and the mixtures were incubated with magnetic beads for 30 min to facilitate. Then, immunoprecipitation of the SV-HUC-1 cell lysates with the antibodies was performed. Finally, the coprecipitated RNA was converted into cDNA through reverse transcription and subsequently analyzed by qPCR, followed by agarose gel electrophoresis for quantitative assessment.

Coimmunoprecipitation (Co-IP)

A total of 1×10^7 control and stable circPDE3B-overexpressing SV-HUC-1 cells were collected, and the experiments were performed using a Co-IP detection kit (BersinBio, Bes3011). First, the cells were lysed to extract proteins, antibodies were conjugated to protein-A/G magnetic beads, and then, the cell protein lysates were added to adsorb the target proteins. The target proteins were subsequently separated from the magnetic beads, and protein samples were collected for western blotting experiments to detect the immunoprecipitated proteins.

Transient overexpression cell transfection

The HIF-1 α overexpression vector (P42543) and its control vector (pCDNA3.1) were obtained from MiaoLingBio. A total number of 3×10^5 cells were plated in six-well plates, and when the cells had attained 70% confluence, they were transfected with LipofectamineTM 3000 Transfection Reagent (Invitrogen, L3000015). LipofectamineTM 3000 Transfection Reagent was used to transfect the overexpression plasmids and vectors into the cells according to the manufacturer's instructions in the appropriate system, and the medium was replaced with complete medium after 8 h. The cells were collected after 48 h for subsequent experiments.

Protein stability assay

Control and stable circPDE3B-overexpressing SV-HUC-1 cells were plated at a density of 3×10^5 cells/well in six-well plates. When the cells reached the logarithmic growth phase, they were exposed to 100 μ g/ml cycloheximide (CHX), the cellular proteins were extracted after 0 h, 3 h, 6 h, and 9 h, and protein expression was measured by western blotting.

Proteasome inhibition assay

Control and stable circPDE3B-overexpressing SV-HUC-1 cells were plated at a density of 3×10^5 in six-well plates and subsequently treated with the proteasome inhibitor MG132 (MedChemExpress, HY-13259-10 mg) at a concentration of 10 μ M. During the logarithmic growth phase, cellular proteins were harvested at 0 h and 24 h, and the expression levels of proteins were analyzed using western blotting.

Western blotting experiment

Cells were disrupted using a with cell lysis buffer containing 10 mM Tris-HCl [pH 7.4], 1% SDS and 1 mM Na_3VO_4 , and the proteins were extracted. The proteins were denatured at 100 °C for 5 min, and then, followed by ultrasonic homogenization of the cell lysates using an ultrasonic cell crusher (Ningbo Scientz Biotechnology Co., Ltd.). The supernatants were centrifuged to obtain the proteins, and the protein concentration were measured using a PierceTM BCA protein assay kit (Thermo Fisher Scientific, 23227) prior to preparing the protein samples were prepared. Protein samples were then separated via sodium dodecyl sulfate–polyacrylamide gel electrophoresis (SDS–PAGE) and subsequently transferred onto polyvinylidene difluoride (PVDF) membranes for 60–120 min at a constant current of 200 mA. The membranes were blocked for 1 h at room temperature with 5% skim milk, and the PVDF membranes were incubated with primary antibodies at 4 °C overnight, followed by incubation with goat anti-mouse IgG (Cell Signaling Technology, Inc., 4408S) or goat anti-rabbit IgG (Cell Signaling Technology, Inc., 8890S) for 1 h at room temperature. Subsequently, chemiluminescence imaging was carried out using a Clinx S6 system, and the grey values of the protein bands were

analysed with ImageJ software. The antibodies that were used in this study targeted the following proteins: NF- κ B (SANTA, sc-8008, 1:500), STAT3 (Proteintech, 60199-1-Ig, 1:2000), HIF-1 α (Proteintech, 20960-1-AP, 1:5000), P21 (Proteintech, 10355-1-AP, 1:2000), and Bcl2 (Proteintech, 803-1-RR, 1:5000).

Prediction of biological function

We visualized and analyzed the differential expression of the high-throughput sequencing results (Gene Expression Omnibus (GEO) database: GSE159239) of the subject group through Wei Sheng Xin (<https://www.bioinformatics.com.cn/>). The circbase (<https://www.circbase.org/>), UCSC (<https://genome.ucsc.edu/>) and CSCD (<http://gb.whu.edu.cn/CSCD/>) websites were used to find circPDE3B (hsa_circ_0000277) sequence and the cyclization site. The circmine database (<http://www.biomedical-web.com/circmine/home>), Targetscan (https://www.targetscan.org/vert_80/) and the DAVID database (<https://david-bioinformatics.nih.gov/>) were utilized for KEGG enrichment analysis of downstream genes of circPDE3B. The downstream targets of NF- κ B and STAT3 were predicted via TRRUST (<https://www.grnpedia.org/trrust/>) and analyzed by jvenn (<https://www.bioinformatics.com.cn/static/others/jvenn/example.html>) to take the intersection of the prediction results for analysis.

Statistical analysis

The results we present have been carried out in three biological replicates, and the experimental data are expressed as the means \pm standard deviations (means \pm SDs). SPSS 23.0 and GraphPad Prism 9.0 software were used to statistically analyse the experimental data and generate the graphs. Two independent samples *t* tests were used for data conforming to a normal distribution, one-way ANOVA was employed for comparing multiple groups, and the rank-sum test was used for samples that did not conform to a normal distribution. * denotes intragroup comparisons, # denotes intergroup comparisons, and $p < 0.05$ indicates that the difference was statistically significant (*, # both indicate $p < 0.05$).

Results

Establishment of a model of SV-HUC-1 cell malignant transformation induced by NaAsO₂ and screening of circPDE3B

To establish a model of the malignant transformation of SV-HUC-1 cells induced by NaAsO₂, SV-HUC-1 cells were exposed to 0, 0.5, 1, 2, 4, 8, or 16 μ M NaAsO₂ for 24 h, 48 h, or 72 h. Cell viability was determined with the CCK-8 assay, the optimal arsenic exposure time for SV-HUC-1 cells was determined to be 48 h (Fig. 1A), and the highest cell viability was observed at a NaAsO₂ concentration of 0.5 μ M (Fig. 1B). SV-HUC-1 cells were continuously treated with 0.5 μ M NaAsO₂ and cultured till 80 generations. Soft agar colony formation assays revealed that malignant proliferation was significantly increased in SV-HUC-1 cells that were treated with 0.5 μ M NaAsO₂ for a long period (Fig. 1C and D). These findings indicate that a model of NaAsO₂-induced malignant transformation in SV-HUC-1 cells was successfully established.

To explore the mechanism by which circRNAs function in the malignant transformation of SV-HUC-1 cells triggered via arsenic, we performed an in-depth analysis of previous high-throughput sequencing results based on previous research from our research group (Wu et al. 2022a, 2022b), and we screened for circRNA-circPDE3B, which was significantly upregulated (Fig. 1E). SV-HUC-1 cells were treated with arsenic for 0 generations (P0), 20 generations (P20), 40 generations (P40) and 80 generations (P80), and the expression levels of circPDE3B were measured. The findings showed circPDE3B exhibited continuous upregulation during the arsenic-induced malignant transformation of SV-HUC-1 cells triggered via arsenic. Therefore, we selected the upregulated gene circPDE3B for subsequent research (Fig. 1F). We searched the UCSC (<https://genome.ucsc.edu/>) and CSCD (<http://gb.whu.edu.cn/CSCD/>) websites for the circularization site of circPDE3B and designed circPDE3B-specific primers for qPCR and Sanger sequencing to confirm that circPDE3B is composed of the reverse splicing and circularization from exons 3 to 6 in chromosome 11 (Fig. 1G). To validate the circular architecture of circPDE3B, we designed convergent and divergent primers. After total cellular RNA was

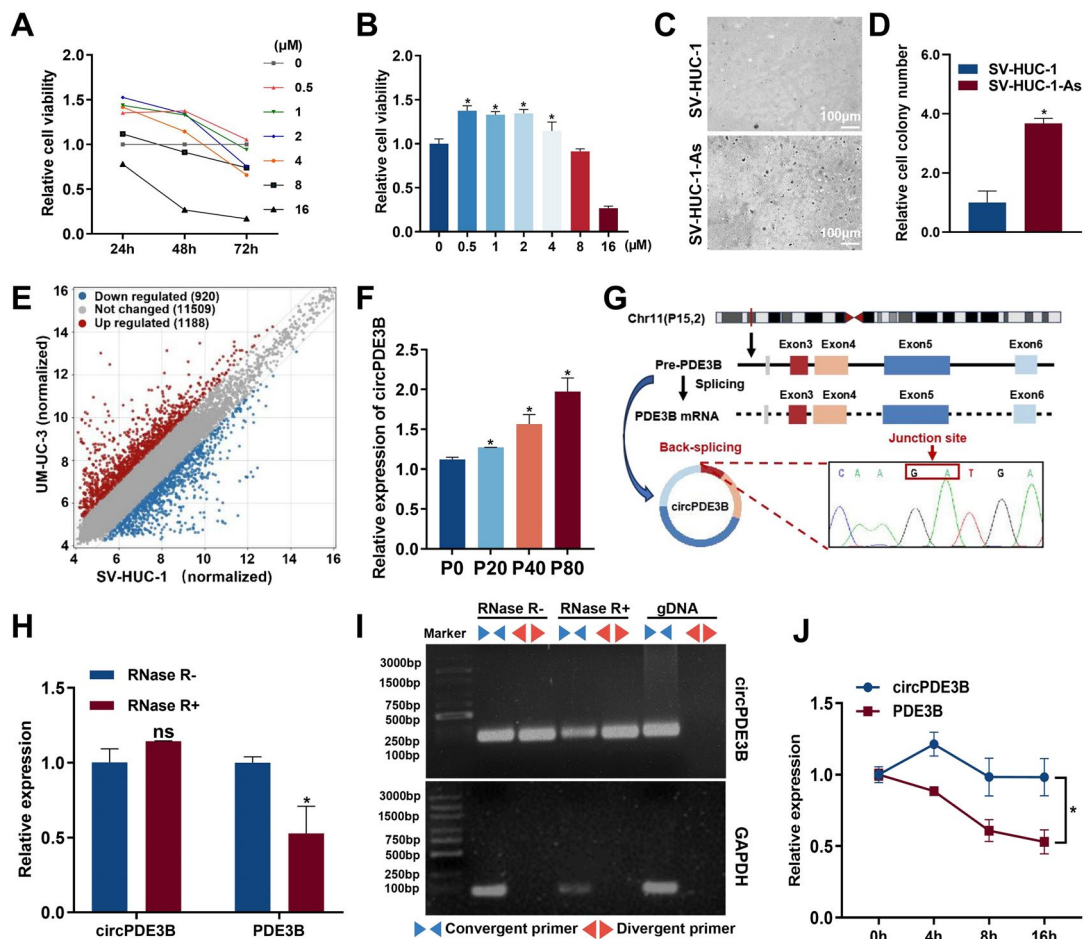
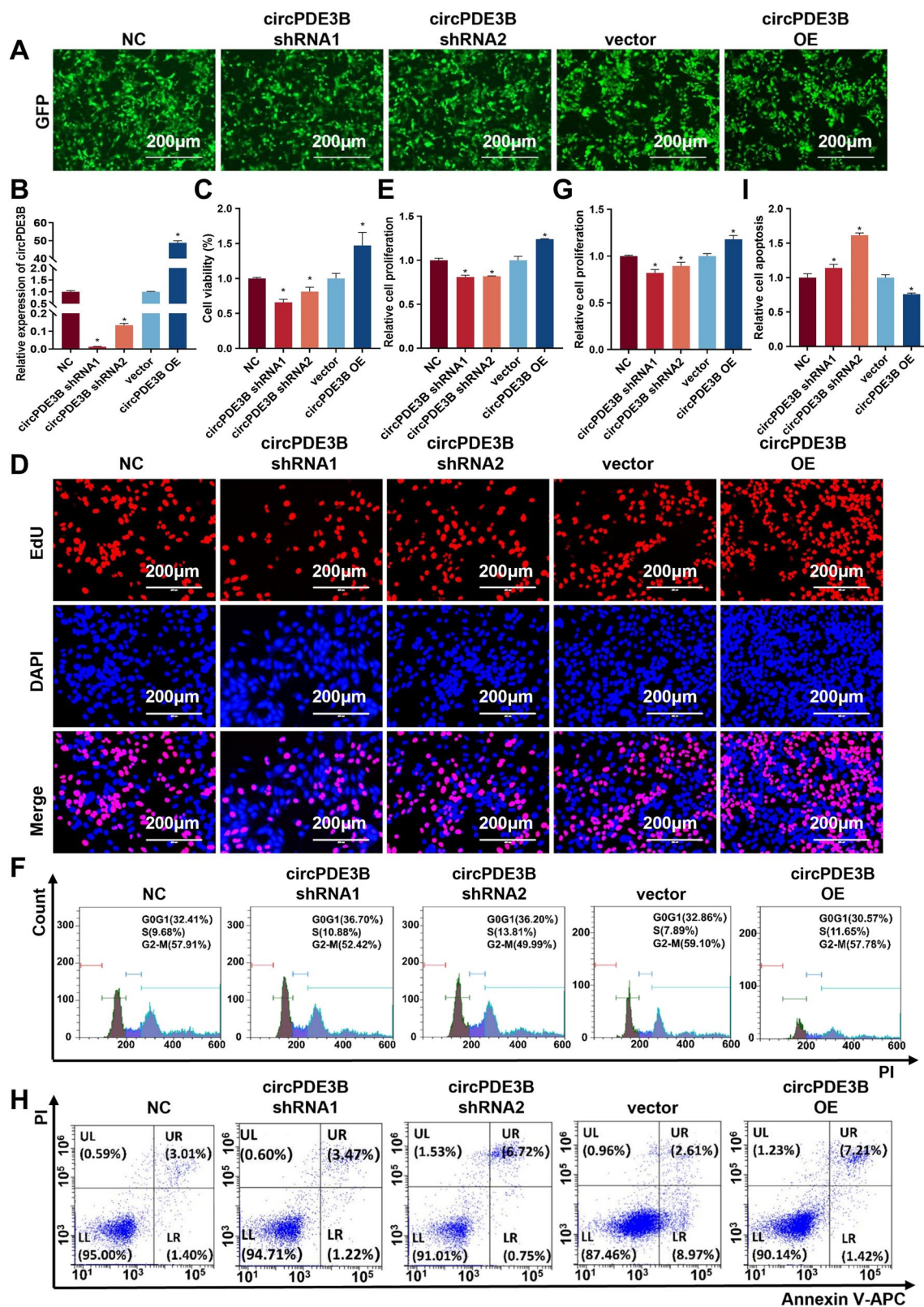


Fig. 1 Establishment of a model of SV-HUC-1 cell malignant transformation induced by NaAsO₂ and screening of circPDE3B. **(A)** The CCK-8 assay to identify changes in cellular viability after exposure to arsenic for different time points and at different concentrations. **(B)** CCK-8 assay to determine cell viability after 48 h of arsenic exposure. **(C)** Soft agar colony formation assay to assess the colony-forming ability of SV-HUC-1 cells cultured for 80 generations with continuous NaAsO₂ exposure. **(D)** Statistical analysis of soft agar colony formation experiments. **(E)** Volcano plots showing the differential expression profiles of circRNAs in SV-HUC-1 cells and UM-UC-3 cells, with red denoting significantly upregu-

lated circRNAs, blue denoting significantly downregulated circRNAs, and grey denoting circRNAs without differential expression. **(F)** qPCR measurement of circPDE3B expression in different generations. **(G)** Schematic diagram of the circPDE3B gene structure. **(H)** circPDE3B and linear PDE3B gene expression before and after RNase R treatment was measured by qPCR. **(I)** Agarose gel electropherograms of polymerization dispersion experiments. **(J)** SV-HUC-1 cells were treated with Act D for 0 h, 4 h, 8 h or 16 h. RNA was extracted for qPCR to measure circPDE3B and linear PDE3B expression. The values are presented as means \pm SDs, and each experiment was performed at least three times. *, $p < 0.05$; ns, $p \geq 0.05$

extracted, linear RNA was digested with RNase R, and changes in circPDE3B and linear PDE3B were measured by RT-qPCR. Agarose gel electrophoresis was carried out. The findings revealed circPDE3B was more tolerant to RNase R digestion than its homologous linear RNA (Fig. 1H and I). To further confirm the stability of circPDE3B, SV-HUC-1

cells were subjected to actinomycin D (Act D) treatment with 0 h, 4 h, 8 h, and 16 h, and total cellular ribonucleic acid was collected for qPCR analysis. The findings demonstrated that circPDE3B exhibited a longer half-life compared to homologous linear RNA (Fig. 1J). These experiments validated the circular structure of circPDE3B.



◀Fig. 2 circPDE3B significantly promotes the proliferation of SV-HUC-1 cells. (A) GFP fluorescence of successfully established SV-HUC-1 cell lines in which circPDE3B was stably silenced or overexpressed. (B) Validation of the stable circPDE3B silencing or overexpression efficiency circPDE3B in cell lines. (C) CCK-8 assay to measure cell viability after circPDE3B was silenced or overexpressed in SV-HUC-1 cells. (D) EdU assay to assess cell proliferation after circPDE3B was silenced or overexpressed in SV-HUC-1 cells. (E) Statistical analysis of cell proliferation as determined by the EdU assay. (F) Flow cytometry analysis of the cell cycle after circPDE3B was silenced or overexpressed in SV-HUC-1 cells. (G) Statistical analysis of cell proliferation after the cell cycle was analysed by flow cytometry. (H) Flow cytometry analysis of cell apoptotic after the silencing and overexpression of circPDE3B in SV-HUC-1 cells. (I) Statistical analysis of apoptosis as analysed by flow cytometry. The values are presented as means \pm SDs, and each experiment was performed at least three times. *, $p < 0.05$

circPDE3B significantly promotes the proliferation of SV-HUC-1 cells

Investigating the biological function of circPDE3B, we constructed a research system to stably silence and overexpress circPDE3B. SV-HUC-1 cells were infected by lentivirus, the GFP fluorescent signal in the cells was subsequently visualised via fluorescence microscope, whilst the expression efficiency was determined by qPCR (Fig. 2A and B). Cell viability after the stable silencing or overexpression of circPDE3B was measured with CCK-8 experiment. Cell viability decreased with circPDE3B silenced and increased with circPDE3B overexpressed (Fig. 2C). The effect of circPDE3B on cell proliferation was assessed with EdU detection and flow cytometry. The findings suggested that cell proliferation decreased after circPDE3B was silenced and increased after circPDE3B was overexpressed (Fig. 2D–G). Influence of circPDE3B to apoptosis was determined via flow cytometry. After circPDE3B was silenced, cell apoptosis increased, and after circPDE3B was overexpressed, cell apoptosis decreased (Fig. 2H and I). These results indicate that circPDE3B can positively regulate cell proliferation and negatively regulate cell apoptosis.

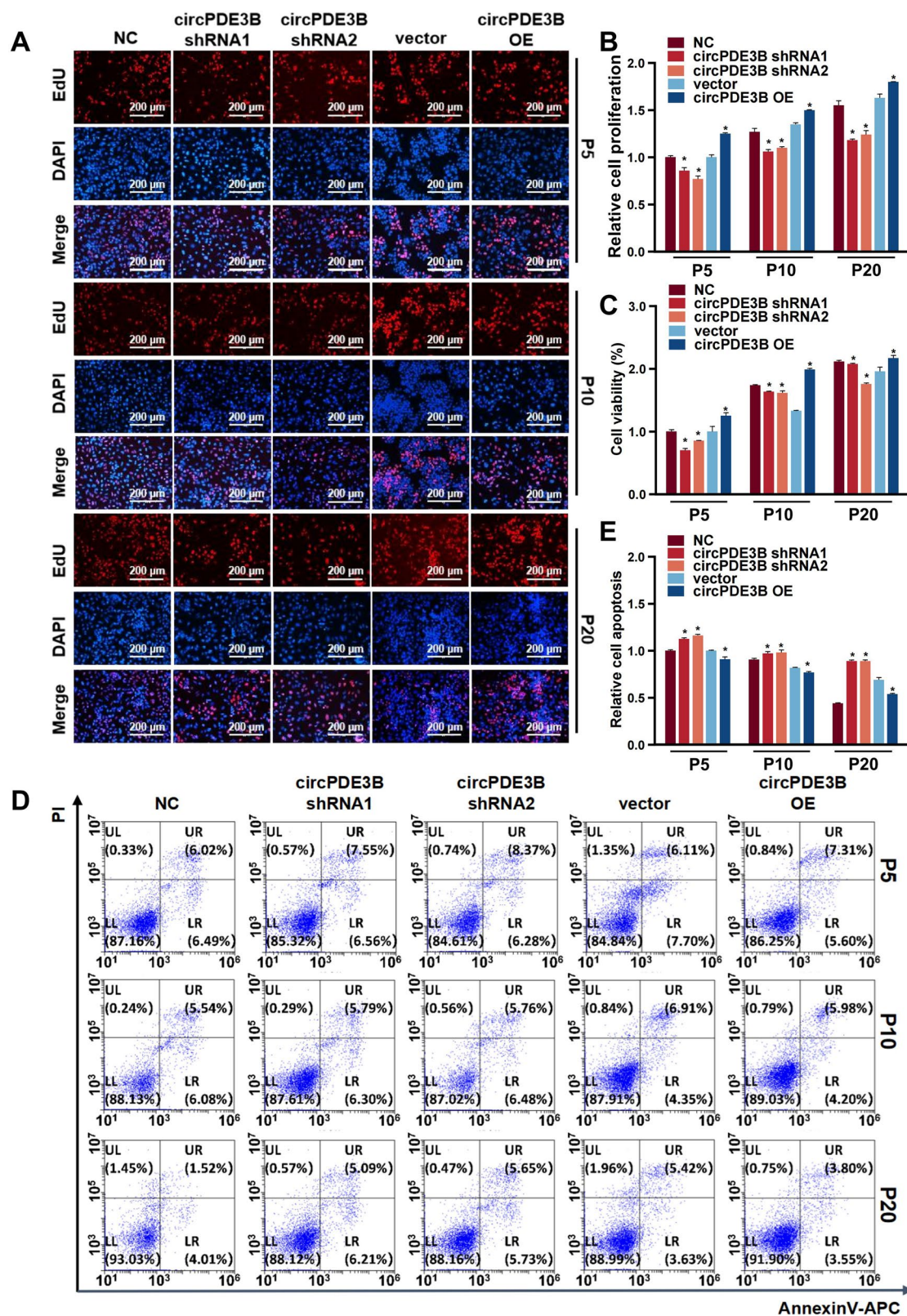
circPDE3B significantly promotes the NaAsO₂-induced malignant transformation of SV-HUC-1 cells

On the basis of the above research, we explored in depth whether circPDE3B could promote the

NaAsO₂-induced carcinogenesis of bladder cancer by affecting cell apoptosis and proliferation. We cultured SV-HUC-1 cell lines circPDE3B in which circPDE3B was stably silenced or overexpressed under conditions of continuous exposure to 0.5 μ M NaAsO₂ and selected cells in the 5th generation (P5), 10th generation (P10) and 20th generation (P20) for grouping experiments. The effect of circPDE3B on cell proliferation under conditions of arsenic exposure was measured with the EdU assay. Compared with that of the control group, cell proliferation increased after circPDE3B was overexpressed, and cell proliferation decreased after circPDE3B was silenced. Furthermore, cell proliferation increased with increasing arsenic exposure (Fig. 3A and B). The effect of circPDE3B on cell viability during arsenic exposure was detected via the CCK-8 experiment. The results revealed that cell viability increased after circPDE3B was overexpressed but decreased after circPDE3B was silenced compared with that of the control group. Moreover, with increasing arsenic exposure, cell viability increased accordingly (Fig. 3C). We also used flow cytometry to observe changes in the ability of circPDE3B to induce apoptosis under conditions of arsenic exposure. As comparison to the control group, the overexpression of circPDE3B enhanced resilience against cells to apoptosis, while the silence of circPDE3B the opposite trend was observed. Furthermore, with increasing arsenic exposure, the resistance of cells to apoptosis increased (Fig. 3D and E). These results show that the expression of circPDE3B increases during the NaAsO₂-induced malignant transformation of SV-HUC-1 cells and that, with increasing arsenic exposure, the proliferation of these cells increases while their apoptosis decreases.

circPDE3B targets and promotes the expression of NF- κ B and STAT3

To explore the molecular mechanism by which circPDE3B functions in the malignant transformation of SV-HUC-1 cells triggered by NaAsO₂, the intracellular distribution of circPDE3B was explored with a nuclear and cytoplasmic fractionation experiment and a FISH experiment. The results indicated that circPDE3B was distributed in both the nucleus and the cytoplasm, but it was located mainly in the cytoplasm (Fig. 4A and B). Therefore, the following experiments were carried out to



◀Fig. 3 circPDE3B significantly promotes the NaAsO₂-induced malignant transformation of SV-HUC-1 cells. **(A)** Stable circPDE3B-silenced and circPDE3B-overexpressing cell lines were exposed to NaAsO₂ for the P5, P10 and P20 generations, and an EdU assay was performed to measure cell proliferation. **(B)** Statistical analysis of cell proliferation as determined by EdU. **(C)** Stable circPDE3B-silenced and circPDE3B-overexpressing cell lines were exposed to NaAsO₂ for the P5, P10, and P20 generations, and the CCK-8 assay was used to measure cell viability. **(D)** Stable circPDE3B-silenced and circPDE3B-overexpressing cell lines were exposed to NaAsO₂ for the P5, P10, and P20 generations, and flow cytometry was performed to analyse of cell apoptosis. **(E)** Statistical analysis of apoptosis as determined by flow cytometry. The values are presented as means \pm SDs, and each experiment was performed at least three times. *, $p < 0.05$

explore whether circPDE3B functions in the cytoplasm by binding to proteins. First, a KEGG enrichment analysis of the genes that are downstream of circPDE3B was performed, and the results revealed that circPDE3B was associated with multiple tumour-related pathways, including the NF- κ B pathway and the JAK-STAT pathway (Fig. 4C). Combining these results with the literature, we know that NF- κ B and STAT3 play critical roles during tumorigenesis and development (Ma et al. 2020; Oh et al. 2023; Pavitra et al. 2023); thus, we hypothesized that circPDE3B may bind to the NF- κ B and STAT3 proteins to affect their expression and thus perform its function. For this reason, we carried out a RIP experiment (Fig. 4D) to explore whether circPDE3B can directly bind to the NF- κ B and STAT3 proteins. The qPCR results and agarose gel electrophoresis findings showed that, in contrast to the IgG group, the IP group (NF- κ B group and STAT3 group) presented greater enrichment of circPDE3B (Fig. 4E-H), suggesting that circPDE3B can directly bind to NF- κ B and STAT3. After circPDE3B was silenced or overexpressed, western blot analysis was conducted to assess the protein expression of NF- κ B and STAT3. The results showed that circPDE3B can positively regulate the NF- κ B and STAT3 expression levels (Fig. 4I-K). To explore the trends in NF- κ B and STAT3 protein expression during the NaAsO₂-induced malignant transformation of SV-HUC-1 cells, we measured the protein expression for NF- κ B and STAT3 from P0, P20, P40 and P80 cells. The results showed that the longer the exposure to arsenic, the more NF- κ B and STAT3 proteins there were (Fig. 4L-N). These

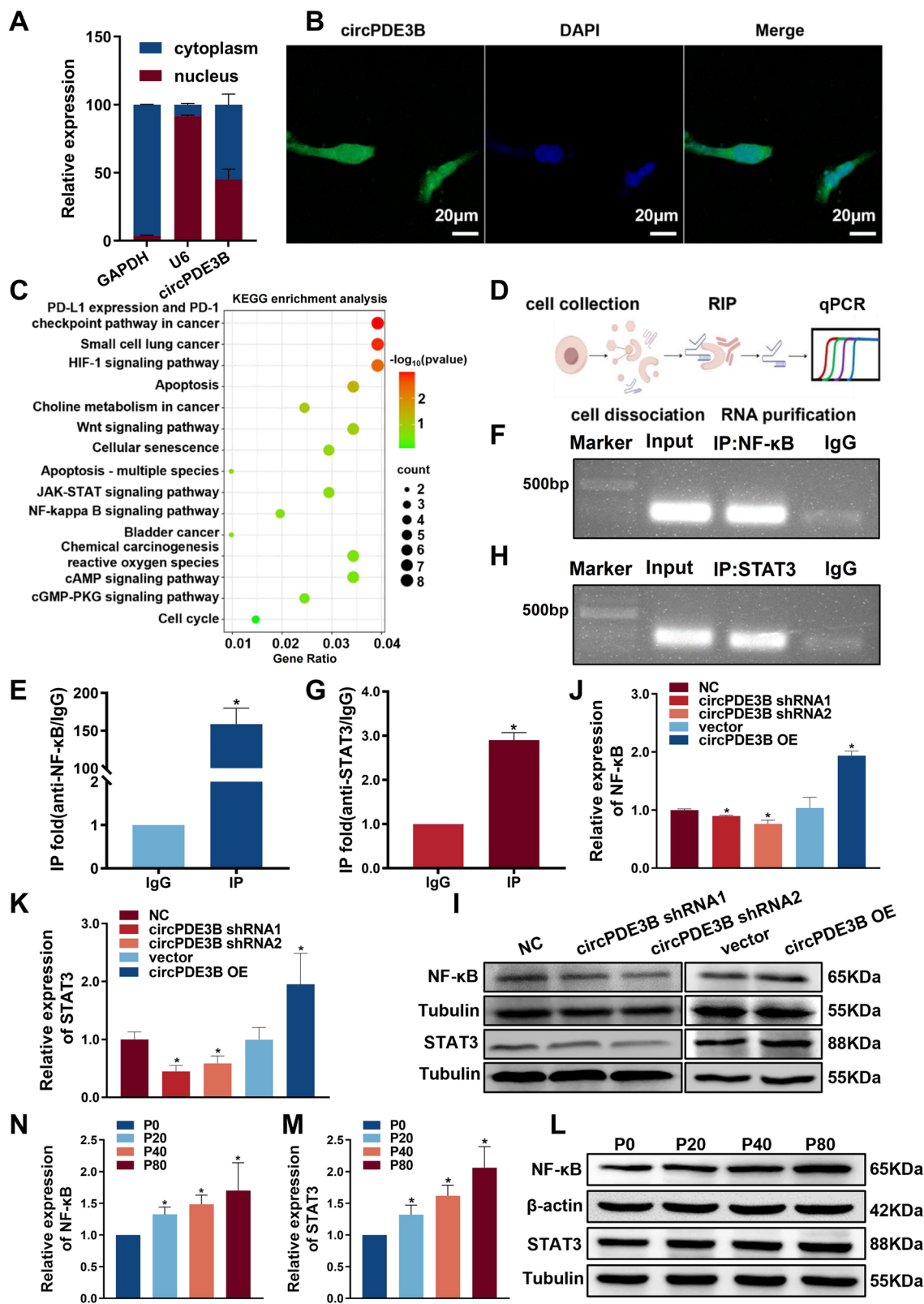
experimental results suggest that circPDE3B can directly bind to the NF- κ B and STAT3 proteins thereby regulating their expression.

circPDE3B inhibits protein degradation by reducing ubiquitination of NF- κ B and STAT3

For the investigation of the effect of circPDE3B on NF- κ B and STAT3, we subjected SV-HUC-1 cells to cycloheximide (CHX) treatment for 0 h, 3 h, 6 h and 9 h to evaluate the stability of NF- κ B and STAT3 after circPDE3B overexpression. The findings suggested that the stability of the NF- κ B and STAT3 proteins was increased after circPDE3B was overexpressed (Fig. 5A-C). The above results indicated that circPDE3B may be associated with degradation of NF- κ B and STAT3, thereby affecting their expression levels. Given that the ubiquitin–proteasome pathway is the main pathway for protein degradation (Liu et al. 2024a; Sun et al. 2024), we further explored whether circPDE3B regulates the ubiquitination of NF- κ B and STAT3 proteins, thus affecting their stability and altering their expression levels. We subjected SV-HUC-1 cells to treatment with the proteasome inhibitor MG132, and we found that MG132 treatment eliminated the impacts of circPDE3B overexpression on the protein levels of NF- κ B and STAT3 proteins (Fig. 5D-F). The results of these experiments revealed that circPDE3B affects the protein degradation of NF- κ B and STAT3 through the proteasome pathway. The results of the coimmunoprecipitation (Co-IP) experiments also revealed that the NF- κ B and STAT3 proteins can bind with ubiquitin proteins and that, as with that in the control group, the binding of ubiquitin proteins in the circPDE3B-overexpressing group was reduced (Fig. 5G and H). These findings suggest that circPDE3B promotes the expression of the NF- κ B and STAT3 proteins through suppression of the ubiquitin–proteasome pathway, reducing the degradation of the NF- κ B and STAT3 proteins and increasing their stability.

circPDE3B regulates HIF-1 α expression through NF- κ B and STAT3

NF- κ B and STAT3 are important transcription factors. We used the TRRUST website (<http://www.grnpedia.org/trrust/>) to predict and analyse the downstream transcription regulatory target genes of NF- κ B and STAT3,



◀Fig. 4 circPDE3B targets and promotes the expression of NF- κ B and STAT3. (A) qPCR detection of the circPDE3B nucleoplasmic distribution in SV-HUC-1 cells. (B) Fluorescence in situ hybridization assay to determine circPDE3B subcellular localization (green fluorescence: circPDE3B; blue fluorescence: nucleus). (C) KEGG pathway enrichment analysis. (D) Schematic diagram of the RIP experiment. (E) RIP-qPCR analysis of circPDE3B directly binding to the NF- κ B protein. (F) Agarose gel electrophoresis of the RIP-qPCR products of circPDE3B directly bound to the NF- κ B protein. (G) RIP-qPCR analysis of circPDE3B directly bound to the STAT3 protein. (H) Agarose gel electrophoresis results of the RIP-qPCR products of circPDE3B directly bound to the STAT3 protein. (I) Western blotting analysis of NF- κ B and STAT3 protein expression after the silencing and overexpression of circPDE3B. (J–K) Statistical analysis of western blotting of NF- κ B protein and STAT3 protein expression. (L) Western blotting analysis of NF- κ B and STAT3 protein expression in the P0, P20, P40 and P80 generations during the NaAsO₂-induced malignant conversion of SV-HUC-1 cells. (M–N) Statistical analysis of NF- κ B and STAT3 protein expression during the NaAsO₂-induced malignant transformation of SV-HUC-1 cells as determined by western blotting. The values are presented as means \pm SDs, and each experiment was performed at least three times. *, $p < 0.05$

and we discovered that NF- κ B and STAT3 can jointly regulate the transcription of HIF-1 α and CCND2 (Fig. 6A). According to the previous KEGG pathway enrichment analysis, circPDE3B is also related to the HIF-1 α pathway. Numerous studies have shown that NF- κ B and STAT3 can cotranscriptionally regulate HIF-1 α expression and affect the protein expression of P21 and Bcl2 to regulate cell proliferation and apoptosis (Jin et al. 2022; Lee et al. 2022; Li et al. 2022a; Nguyen et al. 2023). Therefore, we selected HIF-1 α as a downstream target gene for mechanism exploration. After circPDE3B was silenced or overexpressed in SV-HUC-1 cells, HIF-1 α mRNA expression was measured via qPCR experiment. When circPDE3B was silenced, the expression of HIF-1 α mRNA decreased, and when circPDE3B was overexpressed, HIF-1 α mRNA expression increased (Fig. 6B); these results were consistent with the western blotting results of HIF-1 α protein expression, indicating that circPDE3B positively regulates HIF-1 α (Fig. 6C and D). According to previous studies, circPDE3B can affect SV-HUC-1 cell proliferation and apoptosis. Therefore, after stably silencing and overexpressing circPDE3B, we measured changes in HIF-1 α downstream proteins P21 and Bcl2, which are associated with proliferation and apoptosis, by western blotting. The results showed that circPDE3B negatively regulated P21 protein expression and positively

regulated Bcl2 protein expression (Fig. 6C–F). With increasing duration of NaAsO₂ exposure, the expression level of circPDE3B also enhanced. To explore the changes in the protein expression levels of HIF-1 α , P21 and Bcl2 during the NaAsO₂-induced malignant transformation of SV-HUC-1 cells, western blotting experiments were used to measure the protein expression of HIF-1 α , P21 and Bcl2 in P0, P20, P40 and P80 cells during the arsenic-induced malignant transformation of SV-HUC-1 cells. The results revealed that with increasing arsenic exposure, the protein expression of HIF-1 α and Bcl2 increased, whereas the protein expression of P21 decreased, which was consistent with previous experimental results (Fig. 6G–J). Soft agar colony formation assays with stably circPDE3B-overexpressing SV-HUC-1 cells that were continuously treated with arsenic for 40 generations revealed that circPDE3B accelerated the NaAsO₂-induced malignant transformation of SV-HUC-1 cells (Fig. 6K and Supplementary Fig. 1B). These experiments show that circPDE3B increases the proliferation and inhibits the apoptosis of SV-HUC-1 cells induced by NaAsO₂ by positively regulating HIF-1 α , thereby accelerating the malignant transformation of SV-HUC-1 cells.

circPDE3B promotes the NaAsO₂-induced malignant transformation of SV-HUC-1 cells through the HIF-1 α signalling pathway

To explore whether circPDE3B affects cell proliferation and apoptosis via modulation of the HIF-1 α signalling pathway, we designed a rescue experiment. We constructed a HIF-1 α overexpression plasmid, and we measured HIF-1 α overexpression efficiency by qPCR (Supplementary Fig. 1A). HIF-1 α was overexpressed in cells in which circPDE3B was silenced, and cell viability was assessed using a CCK-8 assay. It was shown that the decrease in cell viability caused by circPDE3B silencing was reversed after HIF-1 α was overexpressed (Fig. 7A). The EdU assay was employed to assess cell proliferation, and the results revealed that the decrease in cell proliferation ability caused by circPDE3B silencing was reversed after HIF-1 α was overexpressed (Fig. 7B and Supplementary Fig. 1C). Apoptosis was measured with flow cytometry, and the findings indicated that overexpressing HIF-1 α counteracted the reduction in resistance to apoptosis caused by circPDE3B silencing (Fig. 7C and Supplementary Fig. 1D). Western blotting was carried

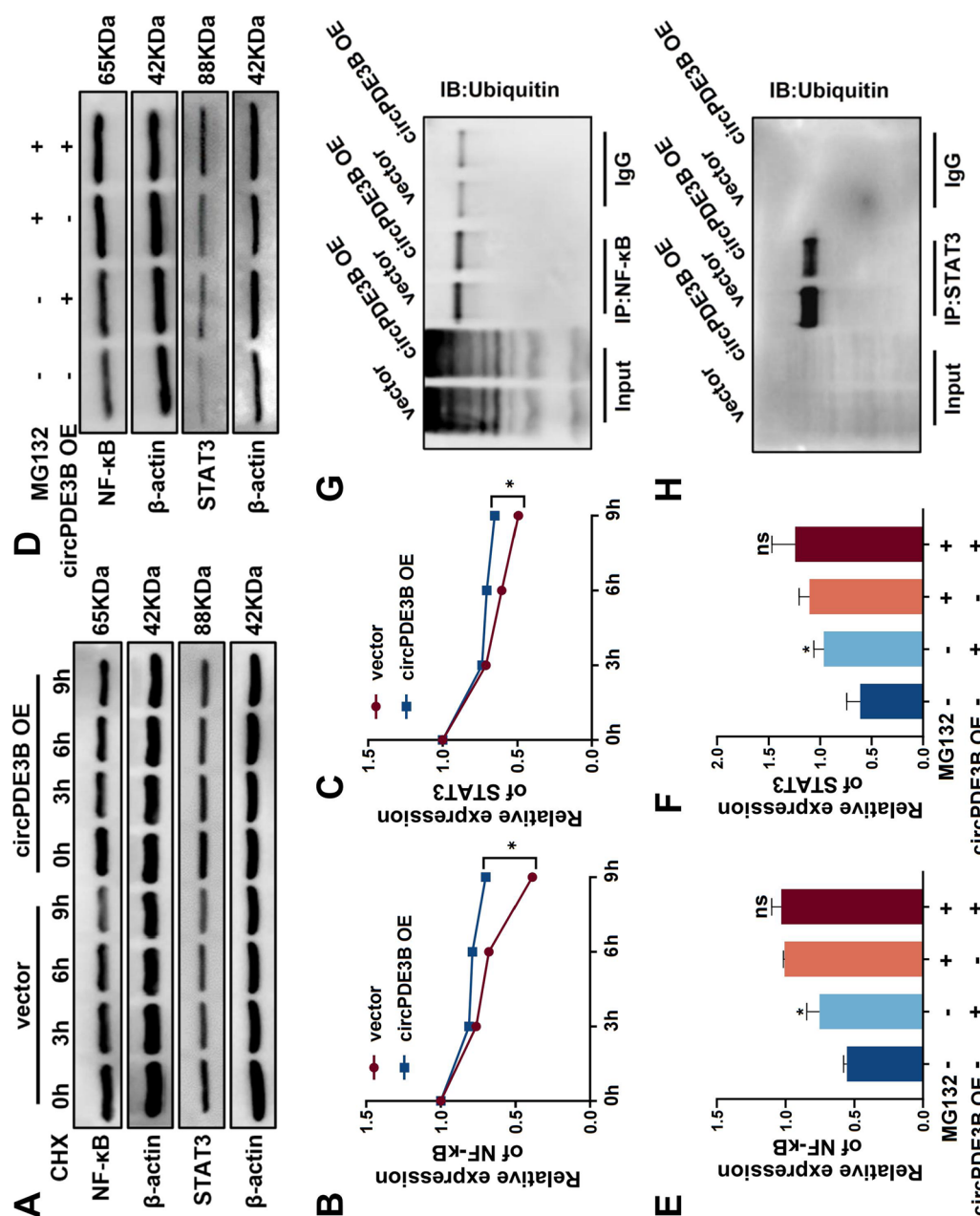


Fig. 5 circPDE3B inhibits protein degradation by reducing the levels of NF-κB and STAT3 ubiquitination. (A) Western blotting was used to measure NF-κB and STAT3 protein expression in stable circPDE3B-overexpressing cells after 0 h, 3 h, 6 h and 9 h of CHX treatment. (B–C) Statistical analysis of NF-κB and STAT3 protein expression after CHX treatment of cells as determined by western blotting. (D) Western blotting was used to measure NF-κB and STAT3 protein expression in stable circPDE3B-overexpressing cells after 10 μM MG132 treatment for 0 h and 24 h. (E–F) Statistical analysis of NF-κB and STAT3 protein expression after MG132 treatment as determined by western blotting. (G) Co-IP assay was conducted to detect the binding of the NF-κB protein and ubiquitin protein. (H) Co-IP assay was conducted to detect the binding of the STAT3 protein and ubiquitin protein. The values are presented as means ± SDs, and each experiment was performed at least three times. *, $p < 0.05$

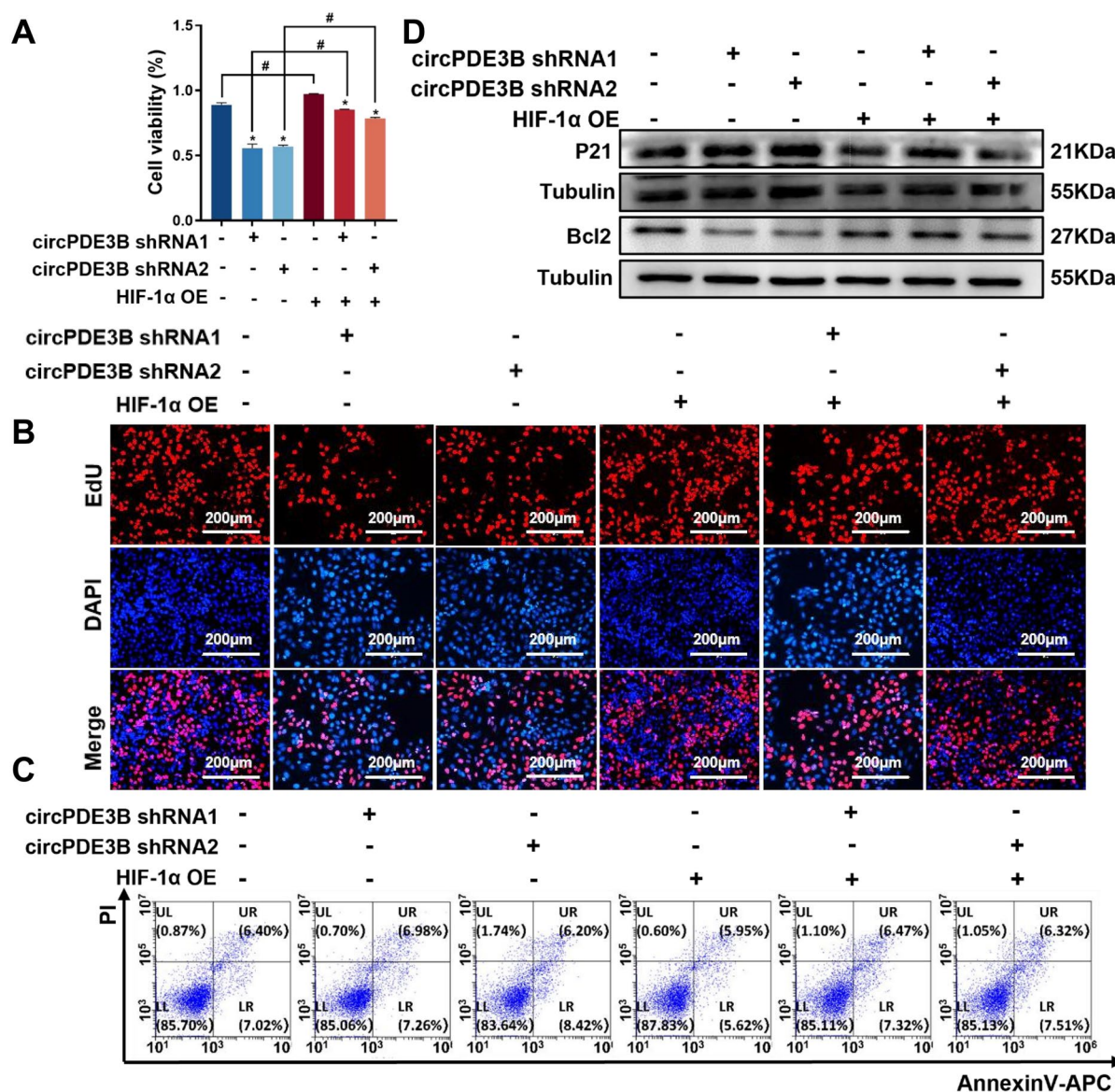


Fig. 7 circPDE3B promotes the NaAsO₂-induced malignant transformation of SV-HUC-1 cells through the HIF-1α signalling pathway. **(A)** CCK-8 assay to determine the viability of circPDE3B-silenced and HIF-1α-overexpressed cells. **(B)** Fluorescence images of circPDE3B-silenced and HIF-1α-overexpressed cells as detected by the EdU assay. **(C)** Flow

cytometry was used to analyse cell apoptosis after circPDE3B was silenced and the HIF-1α was overexpressed. **(D)** Western blotting analysis of P21 and Bcl2 protein expression after circPDE3B was silenced and HIF-1α was overexpressed. The values are presented as means \pm SDs, and each experiment was performed at least three times. *, $p < 0.05$; #, $p < 0.05$

out to measure the changes in the P21 and Bcl2 proteins expression associated with cell proliferation and apoptosis. It was showed the overexpression of HIF-1α reversed the trend of increased P21 protein expression and decreased Bcl2 protein expression caused

by circPDE3B silencing (Fig. 7D and Supplementary Fig. 1E and F). These findings suggest that circPDE3B modulates the HIF-1α signalling pathway, increases cell proliferation, decreases cell apoptosis, promotes the malignant transformation of SV-HUC-1 cells

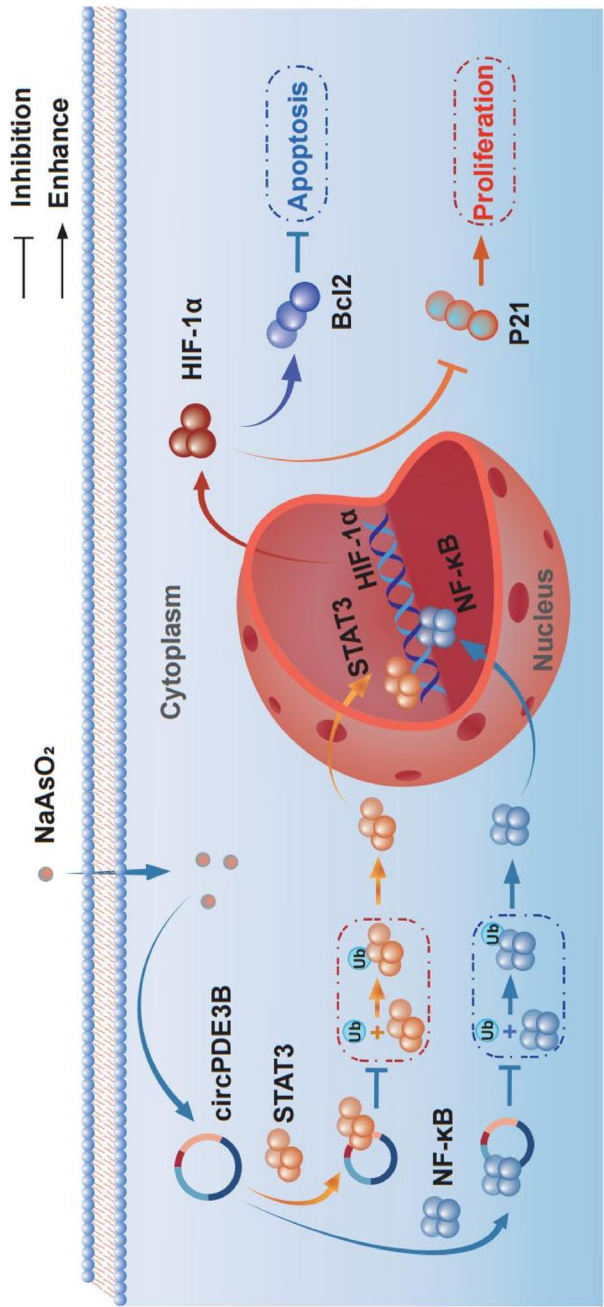


Fig. 8 Mechanism diagram. circPDE3B directly binds to STAT3 and NF-κB to enhance their stability, thereby affecting HIF-1α expression and ultimately promoting arsenic-induced bladder carcinogenesis

triggered via NaAsO_2 , and ultimately leads to bladder carcinogenesis (Fig. 8).

Discussion

In this study, SV-HUC-1 cells were persistently exposed to treatment with low-dose sodium arsenite, and we successfully founded an cell model of transformation triggered via arsenic. We found that circPDE3B expression gradually increased with increasing arsenic exposure, which revealed the molecular mechanism by which circPDE3B targets STAT3 and NF- κ B, decreases their ubiquitination, increases their expression, and then accelerates the malignant transformation of human bladder epithelial cells triggered via arsenic exposure.

Long-term exposure to environmental pollutants has been shown to be one of the leading causes of cancer. Arsenic is a common environmental pollutant that can lead to bladder cancer. The contamination of drinking water by arsenic is the main route of arsenic exposure. Arsenic is mainly present in water bodies in the form of iAs(III) and iAs(V), but iAs(III) is more toxic and prevalent than iAs(V) (Oremland and Stolz 2003). Therefore, we chose continuously expose human bladder epithelial cells to NaAsO_2 . To simulate an environment of chronic arsenic exposure and determine the appropriate conditions for arsenic exposure, we used different time points as well as concentrations, and we found that exposure to arsenic at 0.5 μM for 48 h significantly increased cell viability as shown by a CCK-8 assay; therefore, we chose to culture the cells under these conditions of sustained exposure, and we successfully established a model of the chronic arsenic-triggered malignant transformation of human bladder epithelial cells in the 80th generation. Since it is a long and complex process from early arsenic exposure to bladder carcinogenesis in humans, we hope to find an effective biomarker that can both elucidate the mechanism underlying arsenic-induced bladder carcinogenesis and serve as a diagnostic and therapeutic target during the disease process.

circRNAs have a stable, closed-loop structure, and their expression is affected by exogenous factors in the organism; thus, circRNA molecules have the potential to be used as early diagnostic markers of arsenic-induced bladder carcinogenesis. We used human bladder epithelial cells as the control group and bladder cancer cells as the experimental group,

and we screened for significant differences in the expression of circPDE3B. qPCR experiment showed that the longer the arsenic exposure, the higher the expression of circPDE3B. Through a series of functional experiments, we found that circPDE3B promoted cell proliferation, prevented cell apoptosis, and expedited the arsenic-induced malignant transformation of human bladder epithelial cells. It has been reported that circRNAs can regulate arsenic-induced cancers. For example, circ100284 accelerates the cell cycle to promote the development of skin cancer (Xue et al. 2017); circLRP6 regulates the epithelial–mesenchymal transition occurring in the malignant transformation of human keratinocytes (Xue et al. 2018); and circ008913 acts as a miR-889 sponge that adsorbs DAB2IP and participates in the gain of arsenite CSC-like features that ultimately lead to cell malignant mutation (Xiao et al. 2018). We performed KEGG analysis of circPDE3B to identify signalling pathways that may be regulated by circPDE3B. circPDE3B was found to be significantly enriched in the cancer-related JAK-STAT pathway as well as the NF- κ B pathway. RIP assays revealed that circPDE3B could directly bind to STAT3 and NF- κ B. STAT3 is usually continuously activated in tumour cells, and activated STAT3 can dimerize and subsequently translocate to the nucleus and mitochondria, where it plays roles in transcriptional regulation and the induction of genes associated with tumorigenesis (Gough et al. 2009; Ma et al. 2020; Sun et al. 2023). NF- κ B normally binds to I κ B proteins in the cytoplasm and remains in an inactivated state. When cells are exogenously stimulated, the I κ B protein is degraded, and NF- κ B is freed and moved to the nucleus, where it plays a role in transcriptional regulation (Guo et al. 2024; Liu et al. 2015). Both STAT3 and NF- κ B are reported as activated in several malignant tumours and are involved in tumour development (Yin et al. 2021; You et al. 2023; Zhang et al. 2022; Zhou et al. 2021). Given the important roles of these two proteins in cancer development, an increasing number of studies have explored these two proteins in depth; among these studies, some have shown interactions between STAT3 and NF- κ B. For example, NF- κ B can transcriptionally activate IL-6, and IL-6, which is upstream regulatory factors of STAT3, can promote the sustained activation of STAT3 (Libermann and Baltimore 1990); STAT3 enhances p300-mediated RELA acetylation, prolongs the retention of RELA in the nucleus, and ensures

sustained activation of NF- κ B (Lee et al. 2009). We found that circPDE3B could regulate the levels of STAT3 and NF- κ B ubiquitination, significantly altering their expression. This coregulation of STAT3 and NF- κ B strengthens their interactions during carcinogenesis and promotes cancer development. Despite the progress we have made in our study, shortcomings remain. Notably, STAT3 and NF- κ B act as transcription factors, and their activation involves alterations in phosphorylation; however, our study focused on the level of ubiquitination of these factors and changes in their expression. In the future, we will explore in depth how circPDE3B regulates STAT3 and NF- κ B to more comprehensively understand the key molecular mechanisms underlying carcinogenesis and to clarify the critical function of circPDE3B in tumour.

Given that STAT3 and NF- κ B can be activated and function in coordination with each other in a variety of malignant tumours (He et al. 2022; Zhong et al. 2022), we screened the target genes HIF-1 α and CCNK2, which are regulated by both STAT3 and NF- κ B, via the TRRUST database (<https://www.grnpedia.org/trrust/>). HIF-1 α plays a key role in tumorigenesis and development as a downstream target of STAT3 and NF- κ B, so we selected HIF-1 α as a downstream target gene for further in-depth study. Using a RT-qPCR assay, we found that circPDE3B could regulate the HIF-1 α mRNA levels, suggesting that STAT3 and NF- κ B may act as transcriptional regulators that coregulate HIF-1 α transcription, which is consistent with previously reported findings (Jin et al. 2022; Maimaitiaili et al. 2023; Pawlus et al. 2014; Rius et al. 2008). The specific protein-binding motifs on circRNAs can act as protein decoys, scaffolds and recruiters to enhance interactions between molecules and thus regulate the expression of target genes. Therefore, whether circPDE3B can bind to HIF-1 α and act as a scaffold between STAT3 or NF- κ B and HIF-1 α in order to increase the binding of proteins to DNA and promote HIF-1 α transcription will be further studied in subsequent studies. In summary, our study elucidated the mechanism by which the key regulator circPDE3B functions in arsenic-induced bladder carcinogenesis, providing a new perspective for the prevention of arsenic-induced bladder carcinogenesis and the development of early diagnostic methods.

Author Contributions ARN globally designed and directed this study. GL supervised and gave some advice in this study. YHG and HTX conducted experiments, compiled results,

analyzed data and wrote papers. QYZ, DYC, XDZ, XCC, SYY, DQL, TRN, XYD and MYL provided assistance in completing the experiment and writing the article. ARN guided the revision of this article. All authors reviewed and approved the final manuscript.

Funding This work was partially supported by the National Natural Science Foundation of China (NSFC82260652) and the Natural Science Foundation of Guangxi (2023GXNSFFA026006).

Data availability The sequencing results of the circRNA in this study can be downloaded in the Gene Expression Omnibus (GEO) database (GSE159239).

Declarations

Ethics approval and consent to participate This study did not involve the use of human tissue or the performance of animal experiments.

Consent for publication The contents of this manuscript have not been previously published or considered for publication elsewhere.

Competing interests The authors declare no competing interests.

Open Access This article is licensed under a Creative Commons Attribution-NonCommercial-NoDerivatives 4.0 International License, which permits any non-commercial use, sharing, distribution and reproduction in any medium or format, as long as you give appropriate credit to the original author(s) and the source, provide a link to the Creative Commons licence, and indicate if you modified the licensed material. You do not have permission under this licence to share adapted material derived from this article or parts of it. The images or other third party material in this article are included in the article's Creative Commons licence, unless indicated otherwise in a credit line to the material. If material is not included in the article's Creative Commons licence and your intended use is not permitted by statutory regulation or exceeds the permitted use, you will need to obtain permission directly from the copyright holder. To view a copy of this licence, visit <http://creativecommons.org/licenses/by-nc-nd/4.0/>.

References

- Amara CS, Kami Reddy KR, Yuntao Y, Chan YS, Piyarathna DWB, Dobrolecki LE, Shih DJH, Shi Z, Xu J, Huang S, Ellis MJ, Apolo AB, Ballester LY, Gao J, Hansel DE, Lotan Y, Hodges HC, Lerner SP, Creighton CJ,

- Sreekumar A, Zheng WJ, Msaouel P, Kavuri SM, Putluri N. The IL6/JAK/STAT3 signaling axis is a therapeutic vulnerability in SMARCB1-deficient bladder cancer. *Nat Commun*. 2024;15:1373. <https://doi.org/10.1038/s41467-024-45132-2>.
- Byeon E, Kang HM, Yoon C, Lee JS. Toxicity mechanisms of arsenic compounds in aquatic organisms. *Aquat Toxicol*. 2021;237:105901. <https://doi.org/10.1016/j.aquatox.2021.105901>.
- Chang S, Yim S, Park H. The cancer driver genes IDH1/2, JARID1C/ KDM5C, and UTX/ KDM6A: crosstalk between histone demethylation and hypoxic reprogramming in cancer metabolism. *Exp Mol Med*. 2019;51:1–17. <https://doi.org/10.1038/s12276-019-0230-6>.
- Chen L, Shan G. CircRNA in cancer: Fundamental mechanism and clinical potential. *Cancer Lett*. 2021;505:49–57. <https://doi.org/10.1016/j.canlet.2021.02.004>.
- Dong J, Cheng XD, Zhang WD, Qin JJ. Recent Update on Development of Small-Molecule STAT3 Inhibitors for Cancer Therapy: From Phosphorylation Inhibition to Protein Degradation. *J Med Chem*. 2021;64:8884–915. <https://doi.org/10.1021/acs.jmedchem.1c00629>.
- Gough DJ, Corlett A, Schlessinger K, Wegrzyn J, Larner AC, Levy DE. Mitochondrial STAT3 supports Ras-dependent oncogenic transformation. *Science*. 2009;324:1713–6. <https://doi.org/10.1126/science.1171721>.
- Guldenpfennig C, Teixeira E, Daniels M. NF- κ B's contribution to B cell fate decisions. *Front Immunol*. 2023;14:1214095. <https://doi.org/10.3389/fimmu.2023.1214095>.
- Guo Q, Jin Y, Chen X, Ye X, Shen X, Lin M, Zeng C, Zhou T, Zhang J. NF- κ B in biology and targeted therapy: new insights and translational implications. *Signal Transduct Target Ther*. 2024;9:53. <https://doi.org/10.1038/s41392-024-01757-9>.
- He H, Yi L, Zhang B, Yan B, Xiao M, Ren J, Zi D, Zhu L, Zhong Z, Zhao X, Jin X, Xiong W. USP24-GSDMB complex promotes bladder cancer proliferation via activation of the STAT3 pathway. *Int J Biol Sci*. 2021;17:2417–29. <https://doi.org/10.7150/ijbs.54442>.
- He Z, Wang J, Zhu C, Xu J, Chen P, Jiang X, Chen Y, Jiang J, Sun C. Exosome-derived FGD5-AS1 promotes tumor-associated macrophage M2 polarization-mediated pancreatic cancer cell proliferation and metastasis. *Cancer Lett*. 2022;548:215751. <https://doi.org/10.1016/j.canlet.2022.215751>.
- Jiang N, Liao Y, Wang M, Wang Y, Wang K, Guo J, Wu P, Zhong B, Guo T, Wu C. BUB1 drives the occurrence and development of bladder cancer by mediating the STAT3 signaling pathway. *J Exp Clin Cancer Res*. 2021;40:378. <https://doi.org/10.1186/s13046-021-02179-z>.
- Jin W, Zhao J, Yang E, Wang Y, Wang Q, Wu Y, Tong F, Tan Y, Zhou J, Kang C. Neuronal STAT3/HIF-1 α /PTRF axis-mediated bioenergetic disturbance exacerbates cerebral ischemia-reperfusion injury via PLA2G4A. *Theranostics*. 2022;12:3196–216. <https://doi.org/10.7150/thno.71029>.
- Kristensen LS, Jakobsen T, Hager H, Kjems J. The emerging roles of circRNAs in cancer and oncology. *Nat Rev Clin Oncol*. 2022;19:188–206. <https://doi.org/10.1038/s41571-021-00585-y>.
- Kurosawa A, Saito S, Sakurai M, Shinozuka M, Someya Y, Adachi N. Arsenic affects homologous recombination and single-strand annealing but not end-joining pathways during DNA double-strand break repair. *FEBS J*. 2023;290:5313–21. <https://doi.org/10.1111/febs.16922>.
- Lee H, Herrmann A, Deng JH, Kujawski M, Niu G, Li Z, Forman S, Jove R, Pardoll DM, Yu H. Persistently activated Stat3 maintains constitutive NF- κ B activity in tumors. *Cancer Cell*. 2009;15:283–93. <https://doi.org/10.1016/j.ccr.2009.02.015>.
- Lee SY, Lee AR, Choi JW, Lee CR, Cho KH, Lee JH, Cho ML. IL-17 Induces Autophagy Dysfunction to Promote Inflammatory Cell Death and Fibrosis in Keloid Fibroblasts via the STAT3 and HIF-1 α Dependent Signaling Pathways. *Front Immunol*. 2022;13:888719. <https://doi.org/10.3389/fimmu.2022.888719>.
- Li X, Chen S, Wang X, Zhang R, Yang J, Xu H, He W, Lai M, Wu S, Nan A. The pivotal regulatory factor circBRWD1 inhibits arsenic exposure-induced lung cancer occurrence by binding mRNA and regulating its stability. *Mol Ther Oncolytics*. 2022a;26:399–412. <https://doi.org/10.1016/j.omto.2022.08.006>.
- Li Y, Zheng F, Xiao X, Xie F, Tao D, Huang C, Liu D, Wang M, Wang L, Zeng F, Jiang G. CircHIPK3 sponges miR-558 to suppress heparanase expression in bladder cancer cells. *EMBO Rep*. 2022b;23:e56102. <https://doi.org/10.15252/embr.202256102>.
- Li M, Chen W, Cui J, Lin Q, Liu Y, Zeng H, Hua Q, Ling Y, Qin X, Zhang Y, Li X, Lin T, Huang L, Jiang Y. circ-CIMT Silencing Promotes Cadmium-Induced Malignant Transformation of Lung Epithelial Cells Through the DNA Base Excision Repair Pathway. *Adv Sci (Weinh)*. 2023a;10:e2206896. <https://doi.org/10.1002/adv.202206896>.
- Li YJ, Zhang C, Martincuks A, Herrmann A, Yu H. STAT proteins in cancer: orchestration of metabolism. *Nat Rev Cancer*. 2023b;23:115–34. <https://doi.org/10.1038/s41568-022-00537-3>.
- Libermann TA, Baltimore D. Activation of interleukin-6 gene expression through the NF- κ B transcription factor. *Mol Cell Biol*. 1990;10:2327–34. <https://doi.org/10.1128/mcb.10.5.2327-2334.1990>.
- Liu B, Sun L, Liu Q, Gong C, Yao Y, Lv X, Lin L, Yao H, Su F, Li D, Zeng M, Song E. A cytoplasmic NF- κ B interacting long noncoding RNA blocks IkappaB phosphorylation and suppresses breast cancer metastasis. *Cancer Cell*. 2015;27:370–81. <https://doi.org/10.1016/j.ccell.2015.02.004>.
- Liu F, Chen J, Li K, Li H, Zhu Y, Zhai Y, Lu B, Fan Y, Liu Z, Chen X, Jia X, Dong Z, Liu K. Ubiquitination and deubiquitination in cancer: from mechanisms to novel therapeutic approaches. *Mol Cancer*. 2024a;23:148. <https://doi.org/10.1186/s12943-024-02046-3>.
- Liu Y, Fang S, Lin T, Chen W, Chen Y, Wang Y, Xiao X, Zheng H, Liu L, Zhou J, Jiang Y, Hua Q, Jiang Y. Circular RNA circNIPBL regulates TP53-H179R mutations in NNK-induced bronchial epithelial carcinogenesis. *Environ Int*. 2024b;190:108829. <https://doi.org/10.1016/j.envint.2024.108829>.
- Ma JH, Qin L, Li X. Role of STAT3 signaling pathway in breast cancer. *Cell Commun Signal*. 2020;18:33. <https://doi.org/10.1186/s12964-020-0527-z>.
- Maimaitiali N, Zeng Y, Ju P, Zhakeer G, Yao H, Shi Y, Zhai M, Zhuang J, Peng W, Zhuoga D, Yu Q. NLR3

- deficiency promotes hypoxia-induced pulmonary hypertension development via IKK/NF-kappaB p65/HIF-1alpha pathway. *Exp Cell Res*. 2023;431:113755. <https://doi.org/10.1016/j.yexcr.2023.113755>.
- Mehus AA, Bergum N, Knutson P, Shrestha S, Kalonick M, Zhou X, Garrett SH, Sens DA, Sens MA, Somji S. Chronic Arsenic Exposure Upregulates the Expression of Basal Transcriptional Factors and Increases Invasiveness of the Non-Muscle Invasive Papillary Bladder Cancer Line RT4. *Int J Mol Sci*. 2022;23:12313. <https://doi.org/10.3390/ijms232012313>.
- Muenyi CS, Ljungman M, States JC. Arsenic Disruption of DNA Damage Responses-Potential Role in Carcinogenesis and Chemotherapy. *Biomolecules*. 2015;5:2184–93. <https://doi.org/10.3390/biom5042184>.
- Nguyen V, Zhang Q, Pan F, Jin Q, Sun M, Tangthianchai-chana J, Du S, Lu Y. Zi-Su-Zi decoction improves airway hyperresponsiveness in cough-variant asthma rat model through PI3K/AKT1/mTOR, JAK2/STAT3 and HIF-1alpha/NF-kappaB signaling pathways. *J Ethnopharmacol*. 2023;314:116637. <https://doi.org/10.1016/j.jep.2023.116637>.
- Oh A, Pardo M, Rodriguez A, Yu C, Nguyen L, Liang O, Chorzalska A, Dubielecka PM. NF-kappaB signaling in neoplastic transition from epithelial to mesenchymal phenotype. *Cell Commun Signal*. 2023;21:291. <https://doi.org/10.1186/s12964-023-01207-z>.
- Oremland RS, Stolz JF. The ecology of arsenic. *Science*. 2003;300:939–44. <https://doi.org/10.1126/science.1081903>.
- Pavitra E, Kancharla J, Gupta VK, Prasad K, Sung JY, Kim J, Tej MB, Choi R, Lee JH, Han YK, Raju GSR, Bhaskar L, Huh YS. The role of NF-kappaB in breast cancer initiation, growth, metastasis, and resistance to chemotherapy. *Biomed Pharmacother*. 2023;163:114822. <https://doi.org/10.1016/j.biopha.2023.114822>.
- Pawlus MR, Wang L, Hu CJ. STAT3 and HIF1alpha cooperatively activate HIF1 target genes in MDA-MB-231 and RCC4 cells. *Oncogene*. 2014;33:1670–9. <https://doi.org/10.1038/onc.2013.115>.
- Poma P. NF-kappaB and Disease. *Int J Mol Sci*. 2020;21:9181. <https://doi.org/10.3390/ijms21239181>.
- Porten SP. Epigenetic Alterations in Bladder Cancer. *Curr Urol Rep*. 2018;19:102. <https://doi.org/10.1007/s11934-018-0861-5>.
- Qiu M, Zhang N, Yao S, Zhou H, Chen X, Jia Y, Zhang H, Li X, Jiang Y. DNMT3A-mediated high expression of circ_0057504 promotes benzo[a]pyrene-induced DNA damage via the NONO-SFPQ complex in human bronchial epithelial cells. *Environ Int*. 2022;170:107627. <https://doi.org/10.1016/j.envint.2022.107627>.
- Rius J, Guma M, Schachtrup C, Akassoglou K, Zinkernagel AS, Nizet V, Johnson RS, Haddad GG, Karin M. NF-kappaB links innate immunity to the hypoxic response through transcriptional regulation of HIF-1alpha. *Nature*. 2008;453:807–11. <https://doi.org/10.1038/nature06905>.
- Sassano M, Seyyedsalehi MS, Siea AC, Boffetta P. Occupational arsenic exposure and genitourinary cancer: systematic review and meta-analysis. *Occup Med (Lond)*. 2023;73:275–84. <https://doi.org/10.1093/occmed/kqad066>.
- Speer RM, Zhou X, Volk LB, Liu KJ, Hudson LG. Arsenic and cancer: Evidence and mechanisms. *Adv Pharmacol*. 2023;96:151–202. <https://doi.org/10.1016/bs.apha.2022.08.001>.
- Sun C, Chen Y, Gu Q, Fu Y, Wang Y, Liu C, Xie H, Liao Y, Zheng Z, Liu P, Li M. UBE3C tunes autophagy via ATG4B ubiquitination. *Autophagy*. 2024;20:645–58. <https://doi.org/10.1080/15548627.2023.2299514>.
- Sun Q, Zhao X, Li R, Liu D, Pan B, Xie B, Chi X, Cai D, Wei P, Xu W, Wei K, Zhao Z, Fu Y, Ni L, Dong C. STAT3 regulates CD8+ T cell differentiation and functions in cancer and acute infection. *J Exp Med*. 2023;220:e20220686. <https://doi.org/10.1084/jem.20220686>.
- Tryndyak VP, Borowa-Mazgaj B, Steward CR, Beland FA, Pogribny IP. Epigenetic effects of low-level sodium arsenite exposure on human liver HepaRG cells. *Arch Toxicol*. 2020;94:3993–4005. <https://doi.org/10.1007/s00204-020-02872-6>.
- Virk RK, Garla R, Kaushal N, Bansal MP, Garg ML, Mohanty BP. The relevance of arsenic speciation analysis in health & medicine. *Chemosphere*. 2023;316:137735. <https://doi.org/10.1016/j.chemosphere.2023.137735>.
- Wang D, Chen S, Shao Y, Deng Y, Huang L. EIF4A3 modulated circ_000999 promotes epithelial-mesenchymal transition in cadmium-induced malignant transformation through the miR-205-5p/ZEB1 axis. *Environ Int*. 2024;186:108656. <https://doi.org/10.1016/j.envint.2024.108656>.
- Wu Q, Zhou X, Li P, Ding M, You S, Xu Z, Ye J, Chen X, Tan M, Wang J, Wang W, Qiu J. ROC1 promotes the malignant progression of bladder cancer by regulating p-IkappaBalpha/NF-kappaB signaling. *J Exp Clin Cancer Res*. 2021;40:158. <https://doi.org/10.1186/s13046-021-01935-5>.
- Wu S, Xu H, Zhang R, Wang X, Yang J, Li X, Chen S, He W, Nan A. Circular RNA circLAMA3 inhibits the proliferation of bladder cancer by directly binding an mRNA. *Mol Ther Oncolytics*. 2022a;24:742–54. <https://doi.org/10.1016/j.omto.2022.02.020>.
- Wu S, Yang J, Xu H, Wang X, Zhang R, Lu W, Yang J, Li X, Chen S, Zou Y, Nan A. Circular RNA circGLIS3 promotes bladder cancer proliferation via the miR-1273f/SKP1/Cyclin D1 axis. *Cell Biol Toxicol*. 2022b;38:129–46. <https://doi.org/10.1007/s10565-021-09591-3>.
- Xiao T, Xue J, Shi M, Chen C, Luo F, Xu H, Chen X, Sun B, Sun Q, Yang Q, Dai X, Zhang A, Tang H, Liu Q. Circ008913, via miR-889 regulation of DAB2IP/ZEB1, is involved in the arsenite-induced acquisition of CSC-like properties by human keratinocytes in carcinogenesis. *Metallomics*. 2018;10:1328–38. <https://doi.org/10.1039/c8mt00207j>.
- Xie B, Lin J, Chen X, Zhou X, Zhang Y, Fan M, Xiang J, He N, Hu Z, Wang F. CircXRN2 suppresses tumor progression driven by histone lactylation through activating the Hippo pathway in human bladder cancer. *Mol Cancer*. 2023;22:151. <https://doi.org/10.1186/s12943-023-01856-1>.
- Xue J, Chen C, Luo F, Pan X, Xu H, Yang P, Sun Q, Liu X, Lu L, Yang Q, Xiao T, Dai X, Luo P, Lu J, Zhang A, Liu Q. CircLRP6 Regulation of ZEB1 via miR-455 Is Involved in

- the Epithelial-Mesenchymal Transition During Arsenite-Induced Malignant Transformation of Human Keratinocytes. *Toxicol Sci.* 2018;162:450–61. <https://doi.org/10.1093/toxsci/kfx269>.
- Xue J, Liu Y, Luo F, Lu X, Xu H, Liu X, Lu L, Yang Q, Chen C, Fan W, Liu Q. Circ100284, via miR-217 regulation of EZH2, is involved in the arsenite-accelerated cell cycle of human keratinocytes in carcinogenesis. *Biochim Biophys Acta Mol Basis Dis.* 2017;1863:753–63. <https://doi.org/10.1016/j.bbadis.2016.12.018>.
- Yin H, Zhang X, Yang P, Zhang X, Peng Y, Li D, Yu Y, Wu Y, Wang Y, Zhang J, Ding X, Wang X, Yang A, Zhang R. RNA m6A methylation orchestrates cancer growth and metastasis via macrophage reprogramming. *Nat Commun.* 2021;12:1394. <https://doi.org/10.1038/s41467-021-21514-8>.
- You AB, Yang H, Lai CP, Lei W, Yang L, Lin JL, Liu SC, Ding N, Ye F. CMTR1 promotes colorectal cancer cell growth and immune evasion by transcriptionally regulating STAT3. *Cell Death Dis.* 2023;14:245. <https://doi.org/10.1038/s41419-023-05767-3>.
- Yu H, Lin L, Zhang Z, Zhang H, Hu H. Targeting NF-kappaB pathway for the therapy of diseases: mechanism and clinical study. *Signal Transduct Target Ther.* 2020;5:209. <https://doi.org/10.1038/s41392-020-00312-6>.
- Zhang W, Gong M, Zhang W, Mo J, Zhang S, Zhu Z, Wang X, Zhang B, Qian W, Wu Z, Ma Q, Wang Z. Thiostrepton induces ferroptosis in pancreatic cancer cells through STAT3/GPX4 signalling. *Cell Death Dis.* 2022;13:630. <https://doi.org/10.1038/s41419-022-05082-3>.
- Zhong W, Wu K, Long Z, Zhou X, Zhong C, Wang S, Lai H, Guo Y, Lv D, Lu J, Mao X. Gut dysbiosis promotes prostate cancer progression and docetaxel resistance via activating NF-kappaB-IL6-STAT3 axis. *Microbiome.* 2022;10:94. <https://doi.org/10.1186/s40168-022-01289-w>.
- Zhou J, Dong C, Tan J, Wang G, Li Z, Li S, He Z. Promoting effect and immunologic role of secretogranin II on bladder cancer progression via regulating MAPK and NF-kappaB pathways. *Apoptosis.* 2024;29:121–41. <https://doi.org/10.1007/s10495-023-01898-2>.
- Zhou Q, Tian W, Jiang Z, Huang T, Ge C, Liu T, Zhao F, Chen T, Cui Y, Li H, Yao M, Li J, Tian H. A Positive Feedback Loop of AKR1C3-Mediated Activation of NF-kappaB and STAT3 Facilitates Proliferation and Metastasis in Hepatocellular Carcinoma. *Cancer Res.* 2021;81:1361–74. <https://doi.org/10.1158/0008-5472.CAN-20-2480>.
- Zou S, Tong Q, Liu B, Huang W, Tian Y, Fu X. Targeting STAT3 in Cancer Immunotherapy. *Mol Cancer.* 2020;19:145. <https://doi.org/10.1186/s12943-020-01258-7>.

Publisher's Note Springer Nature remains neutral with regard to jurisdictional claims in published maps and institutional affiliations.